7. C.-M. Tsai, S.-Y. Lee, and H.-M. Lee, Transmission-line filters with capacitively loaded coupled lines, IEEE Trans Microwave Theory Tech 51 (2003), 1517–1524.
8. J.-S. Hong and M.J. Lancaster, Couplings of microstrip square open-loop resonators for cross-coupled planar microwave filters, IEEE Trans Microwave Theory Tech 44 (1996), 2099–2109.

DESIGN OF ULTRA-WIDE STOP-BAND DGS LOW-PASS FILTER USING MEANDER- AND MULTILAYER-TECHNIQUES

M. Al Sharkawy,[1] A. Boutejdar,[2] and E. Galal[1]
[1] Department of Electronics and Communication Engineering, Arab Academy for Science, Technology & Maritime Transport, Alexandria, Egypt
[2] Department of Microwave and Communication Engineering, University of Magdeburg, Universitätsplatz 02 39106, Magdeburg, Germany; Corresponding author: mohamed_sharko1@hotmail.com

Received 22 September 2012

ABSTRACT: *This article presents a new dog-bone defected ground structure (DGS) for low-pass filter (LPF) applications with wide-rejection band and low-insertion loss in the pass-band region. The prototype LPF consists of three dog-bone cells in the ground plane with an open stub on the top layer acting as a compensated capacitor. The prototype LPF is then realized as a multilayer structure to enhance the filter response and reduce its size. The size reduction of the proposed multilayer LPF is about 34% more than the conventional one. The proposed filter has been fabricated and measured. Good agreement can be realized between the electromagnetic simulation and the measurement results. To minimize the difference between the simulation and measurement results, and at the same time to reduce the loss in the pass-band region, a modification to the topology of the structure with the aid of the meander idea is used. The meander-filter presents advantages of compactness, low insertion loss, and high out-band suppression. The dog-bone DGS cell is then used as a photonic band gap structure to minimize the coupling between two probe-fed patch antennas and to improve the two antenna element array efficiency.* © 2013 Wiley Periodicals, Inc. Microwave Opt Technol Lett 55:1276–1281, 2013; View this article online at wileyonlinelibrary.com. DOI 10.1002/mop.27541

Key words: *low-pass filter; defected ground structure; meander*

1. INTRODUCTION

Defected ground structure (DGS) has drawn a great interest in microwave and millimeter wave applications because of its numerous advantages like circuitry size reduction and spurious response suppression. DGS is realized by etching defected pattern or slot in the ground plane. The DGS slot exhibits a band gap characteristic at certain frequency by disturbing the current distribution in the ground plane. This affects the value of the capacitance and inductance of the transmission line [1].

Usually, conventional microwave filters are designed using either shunt stubs or series connected high–low stepped impedance microstrip lines [2–5]. However, this is not applicable for microwave bands because of high-impedance microstrip line and spurious waves. To overcome these disadvantages, DGS patterns and compensated microstrip line are used to design low-pass filter (LPF). Experimental results show that reducing the length and increasing the width of microstrip line is the key to avoid the high impedance in conventional filters.

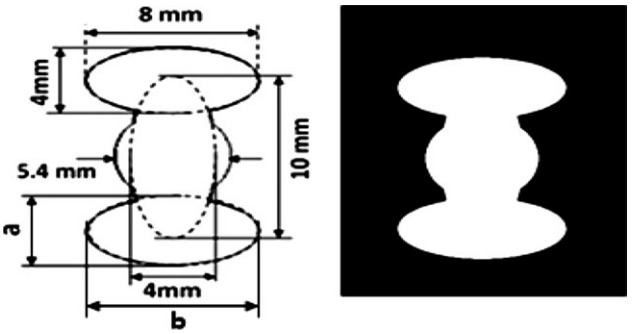

Figure 1 Geometry of a single element for the proposed DGS LPF

In this article, a new compact microstrip dog-bone DGS LPF is proposed with wider and deeper stop-band than those of conventional low-pass filters [5, 6. It is designed to reach a good performance in both pass and stop-bands. The filter has been designed, fabricated, and measured. The measurement results show relatively good agreement with the simulation results. A small deviation is seen between both the results. This deviation can be avoided using the meander idea. Furthermore, the dog-bone DGS cell is then used as a photonic band gap (PBG) structure to reduce the coupling between two probe-fed patch antennas.

2. PROPOSED LOW-PASS FILTER STRUCTURE

2.1. Proposed Dog-Bone DGS Single Element Structure

Figure 1 illustrates the geometry of a single dog-bone DGS element for the proposed LPF. The single DGS element consists of two mirrored elliptical slots of a major radius of 4 mm connected with an ellipse of major radius 5 mm and a circle of radius 2.7 mm instead of a rectangular slot [7] at the center of the DGS element. The proposed DGS slot is etched on a dielectric substrate with relative permittivity 2.2 and a thickness of 0.78 mm. A 50 Ω microstrip line of width 2.421 mm and a compensated capacitance are printed on the top layer as shown in Figure 2. Figure 3 represents the effect of changing the minor and major radii of the ellipse configuration in the dog-bone element, on the S_{11} and S_{21} results. Both radii are related to each other by a factor of 2. One can notice from the S_{11} results of Figure 3 that the pass-band region is at a level of −12 dB, while the rejection band for the LPF starts at 7 GHz as represented by the S_{21} data. It is also clear that there is no significant change, when the ellipse minor diameter (a) increases beyond the 4 mm.

2.2. Prototype LPF Structure

The proposed prototype LPF consists of a 50 Ω microstrip line of width 2.421 mm and a compensated capacitance constructed on the top of dielectric substrate with dimensions of 42 × 27

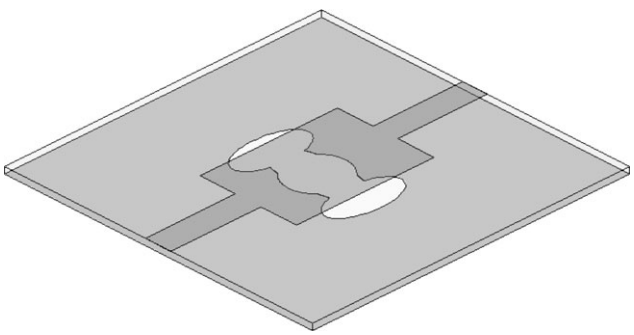

Figure 2 Geometry of a single element for the proposed DGS LPF with compensated capacitor

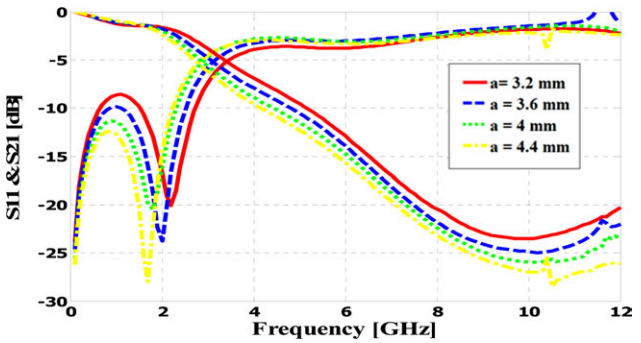

Figure 3 Effect of changing the ellipse radii on both the S_{11} and S_{21} results for the single DGS LPF element. [Color figure can be viewed in the online issue, which is available at wileyonlinelibrary.com]

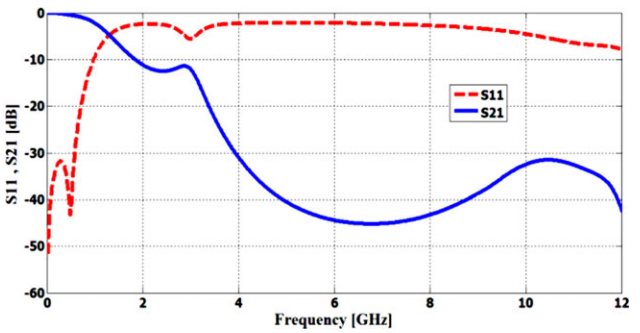

Figure 5 The EM simulation results of the proposed prototype LPF. [Color figure can be viewed in the online issue, which is available at wileyonlinelibrary.com]

mm^2 and relative dielectric constant of 2.2 and a thickness of 0.78 mm as shown in Figure 4. The EM simulation results of the proposed LPF are generated using Ansoft HFSS^{TM} and shown in Figure 5. From Figure 5, it is clearly observed that the attenuation level is equal to -45.23 dB at 6.75 GHz with a minimum reflection of -1.7 dB. A rejection band of 7 GHz can be observed with an overall -20 dB attenuation from a frequency range of 3 to 12 GHz. The proposed prototype LPF is then realized using the multilayer concept to enhance the filter performance and to achieve further size reduction.

2.3. Multilayer LPF with Wide Rejection Band

The multilayer technique is introduced to minimize the size of the proposed prototype LPF [6]. The capacitance on the top layer is replaced by one of the dog-bone DGS elements from the ground plane. This leads to a new compact low-pass filter that consists of a 2.42 mm feed line connected with one dog-bone microstrip patch on the top layer. A total size reduction of 34% was achieved relative to the conventional prototype LPF presented in Figure 4. Figure 6 shows a three-dimensional schematic diagram of the proposed LPF indicating the new dimensions of both, top and bottom layers, with a dielectric substrate size of 34 $\times$ 22 mm^2. The proposed multilayer LPF was fabricated and measured. A picture of the fabricated LPF is presented in Figure 7, which shows the filter top and bottom layers. The simulated and measured frequency responses are shown in Figure 8. Good agreement between the measured and simulated results can be observed. Based on the simulated and measured results one can realize that the proposed multilayer LPF has better performance with a 34% size reduction when compared to the prototype LPF shown in Figure 4.

The coupling distance between the dog-bone DGS elements in the ground plane affects the ripples level in the pass-band region of the proposed LPF as shown in Table 1. It was noticed from the table that at $d = 12$ mm; the ripple level in the pass-band region reaches an optimum value of -18.74 dB with no effect on the size of the filter.

3. ELECTRIC FIELD DISTRIBUTION

A verification of the performance of the proposed DGS LPF using near field distribution has been computed using an EM simulation at three frequencies, one in the pass-band and two at the stop-band regions as shown in Figure 9. It is shown that at frequency $f = 1$ GHz, the electric field is mostly concentrated in the region between the two dog-bone DGS slots in the ground plane and in the dog-bone printed patch on the top layer. Conversely, at frequencies $f = 4$ GHz and $f = 6$ GHz minimum electric field distribution is shown in the DGS slots.

4. IMPROVEMENT OF LOW-PASS FILTER CHARACTERISTICS USING MEANDER IDEA

Figure 10 shows a new topology of DGS- low-pass filter (LPF) with meander 50-Ω microstrip line [8]. As discussed earlier, the filter structure consists of two coupled DGS resonators etched in the ground plane, which is electromagnetic coupled with the top microstrip resonator. The top resonator is connected with both ports through a 50-Ω line. The meander elements are distributed between both ports and the compensated top resonators. As shown in Figure 10, using meander lines cause an additional inductive effect (electromagnetic effect), which reduces the losses in the pass-band and minimizes the shift between the simulation and the experiment results. A new geometry of the feed line is

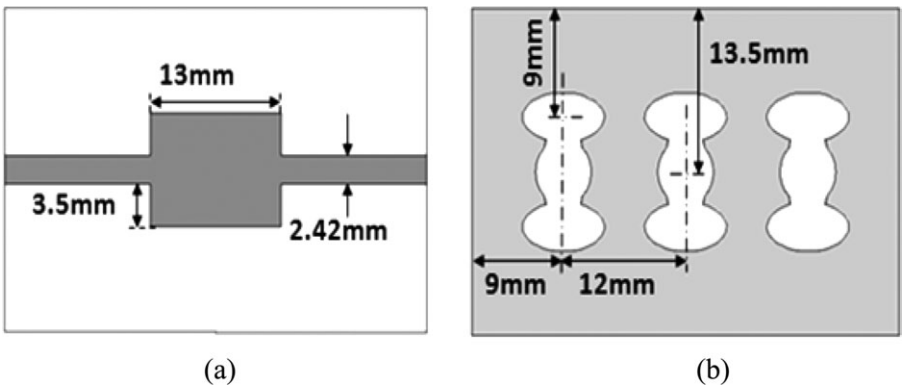

Figure 4 Schematic diagram of the prototype LPF, (a) top layer and (b) bottom layer

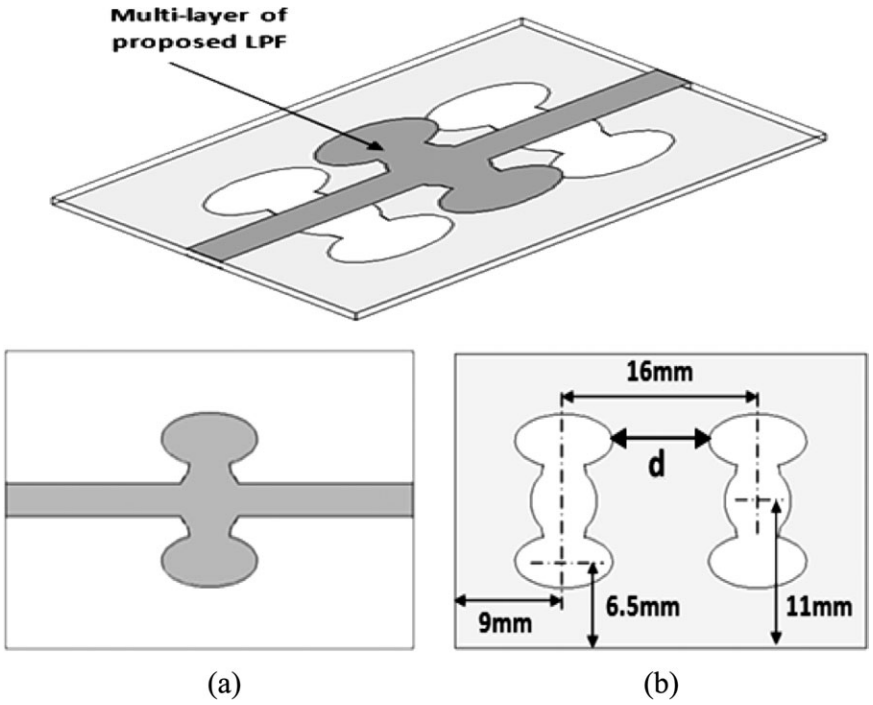

Figure 6 Schematic diagram of multilayer LPF, (a) top layer and (b) bottom layer

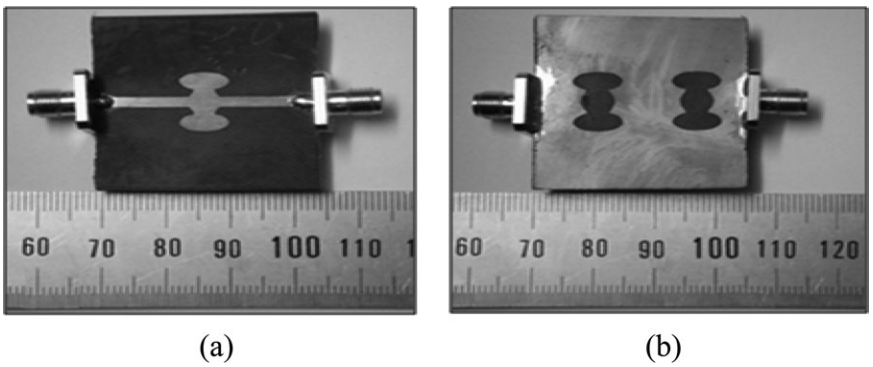

Figure 7 Fabricated DGS-LPF: (a) top view and (b) bottom view

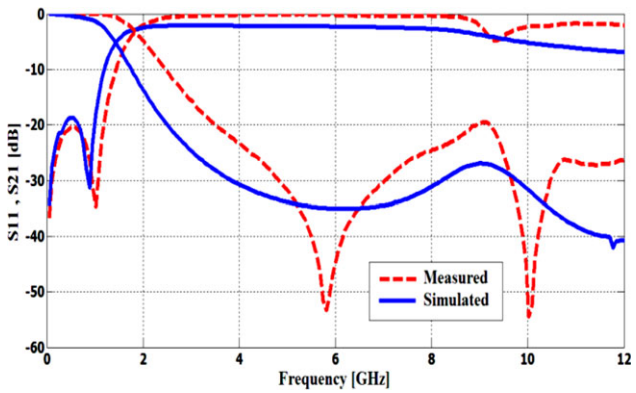

Figure 8 Comparison between simulated and measured results of the dog-bone multilayer LPF. [Color figure can be viewed in the online issue, which is available at wileyonlinelibrary.com]

created and Figure 11 shows the EM simulation results for the new meander DGS low-pass filter.

One can notice, that employing the meander trick leads to an approximation between the simulation and measurement responses. Moreover, the return loss S_{11} reaches −24 dB instead

TABLE 1 The effect of changing the coupling distance on the ripple level in the pass-band region

Coupling distance, d (mm)	Ripple level in pass band (dB)	Size (mm^2)
7	−16.78	34 × 22
8	−16.88	34 × 22
9	−18.24	34 × 22
10	−17.44	34 × 22
11	−17.79	34 × 22
12	−18.74	34 × 22
13	−18.79	36 × 22

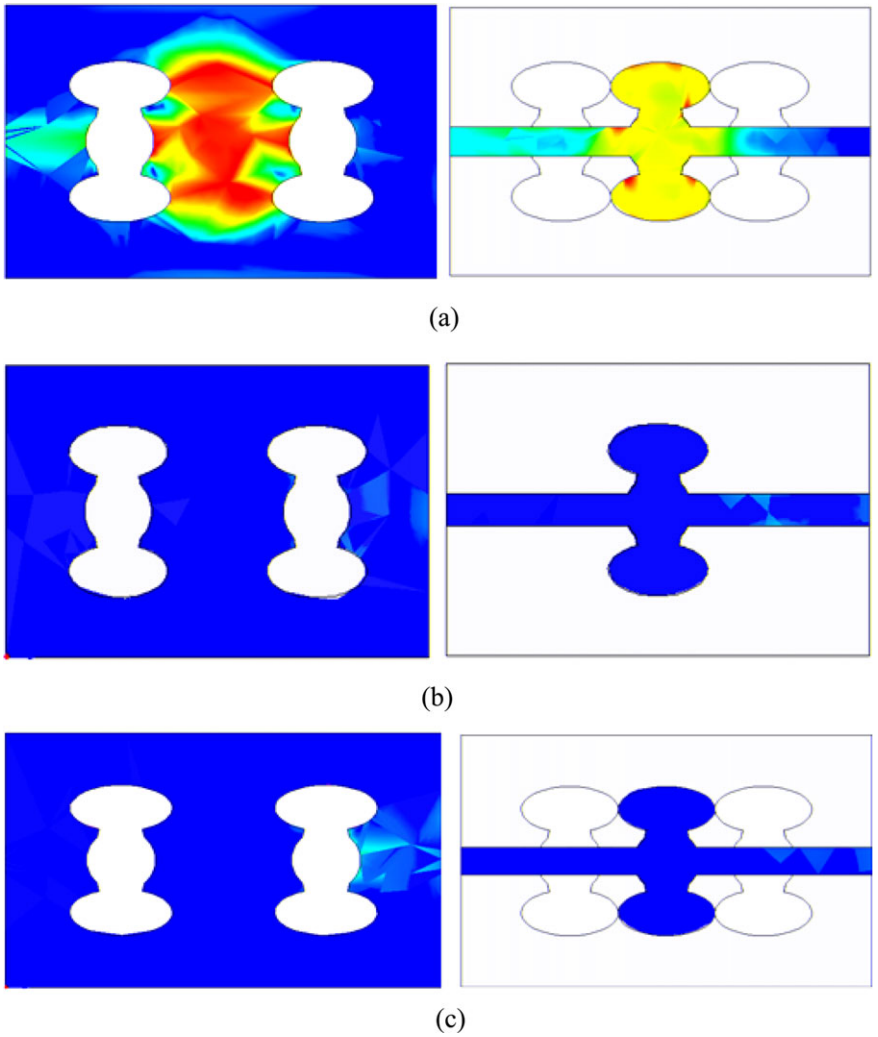

Figure 9 Electric field distribution of the multilayer LPF at: (a) $f = 1$ GHz, (b) $f = 4$ GHz, and (c) $f = 6$ GHz. [Color figure can be viewed in the online issue, which is available at wileyonlinelibrary.com]

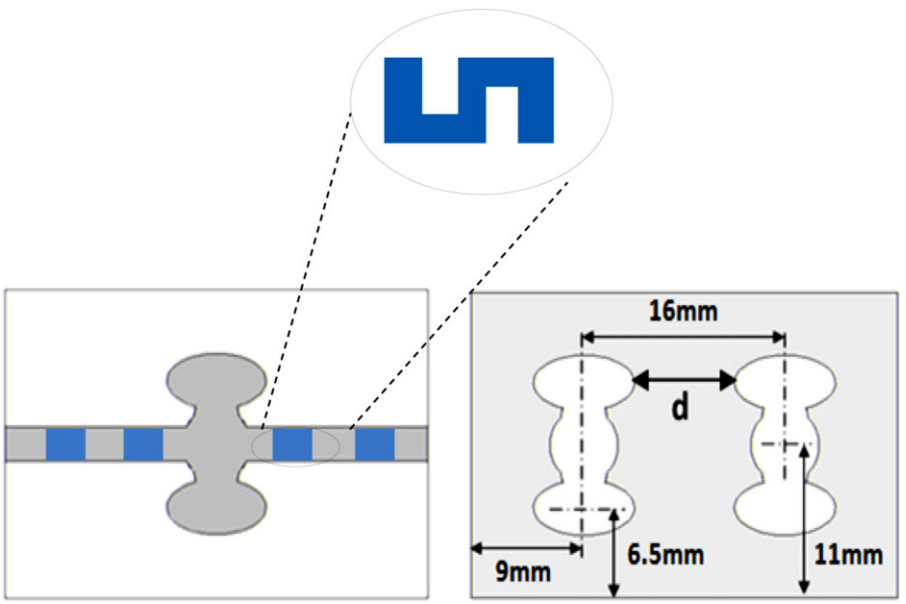

Figure 10 The proposed compact meander DGS low-pass filter. [Color figure can be viewed in the online issue, which is available at wileyonlinelibrary.com]

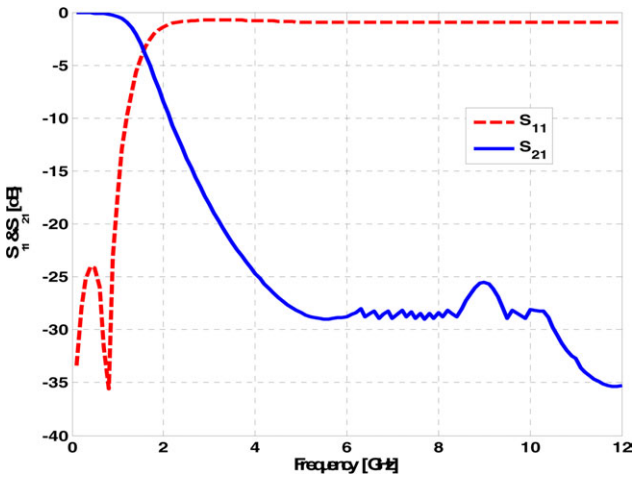

Figure 11 The simulated results of the dog-bone multilayer meander DGS-LPF. [Color figure can be viewed in the online issue, which is available at wileyonlinelibrary.com]

of −20 dB. Further investigation is to be carried on to achieve a better response.

5. PHOTONIC BAND GAP USING DOG-BONE DGS ELEMENT

Microstrip patch antennas have some limitations such as low gain, limited bandwidth, and low radiation efficiency due to surface waves losses. Photonic band gap has the ability to

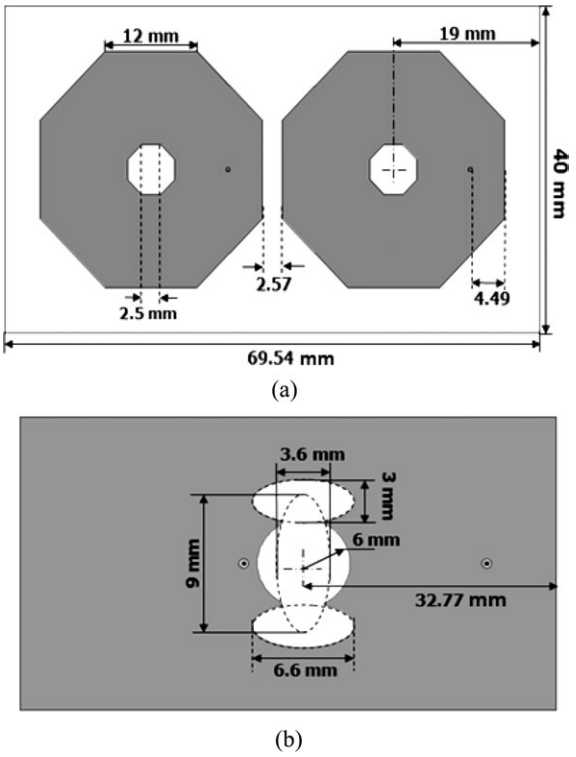

Figure 12 Geometry of two octagonal microstrip patch antennas: (a) top layer and (b) bottom

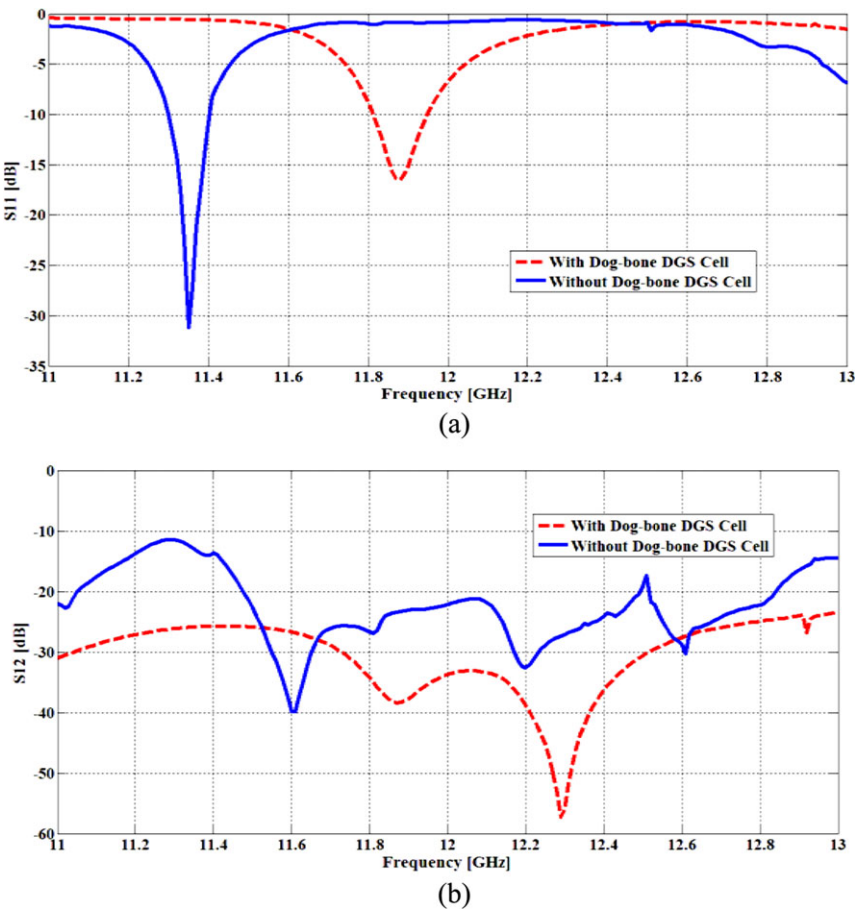

Figure 13 Comparison between the two cases with and without the dog-bone DGS cell for (a) S_{11} and (b) S_{12} results. [Color figure can be viewed in the online issue, which is available at wileyonlinelibrary.com]

minimize the surface waves and enhance the radiation performance. In this section, a PBG is used to minimize the mutual coupling in a closely packed octagonal microstrip patch antennas fed with a coaxial probe. Figure 12 shows the geometry of the proposed octagonal patch antenna indicating all the dimensions of both, top and bottom layers. The frequency response of the octagonal microstrip patch antennas, with and without the PBG structure, is shown in Figure 13. It is clearly observed that the level of mutual coupling between the two octagonal patches has been decreased by almost 10 dB compared to the one without the dog-bone DGS cell [9].

6. CONCLUSION

In this paper, a dog-bone DGS structure has been introduced and investigated for the design of LPF. Simulation shows good consistency with experimental results. The proposed DGS filter is realized as a multilayer LPF to reduce the size and enhance the performance of the prototype LPF. The advantage of using the multilayer technique provides the LPF with around 34% compactness relative to the prototype design. The proposed filter structure has been modeled using electromagnetic simulation. The small deviation between both results and the undesired losses in pass band are due to the fabrication error and the matching error, respectively. To compensate this frequency difference and to improve the pass-band characteristics, a simple modification meander has been used on the 50-Ω line. Further investigation was conducted to study the effect of using the dog-bone DGS element as PBG structure to minimize the mutual coupling between a closely packed octagonal patch antennas fed by a coaxial probe. The simulation results show almost 10 dB mutual coupling reduction between the octagonal microstrip patch antennas after using the proposed dog-bone DGS element.

REFERENCES

1. J.S. Lim, C.-S. Kim, Y.-T. Lee, D. Ahn, and S. Nam, Design of lowpass filters using defected ground structure and compensated microstrip line, Electronic Lett, 38 (2002), 1357–1358.
2. F. Zhang, J. Gu, L. Shi, C. Li, X. Sun, Design of UWB lowpass filter using a novel defected ground structure, Microwave Opt Technol Lett 48 (2006), 1805–1807.
3. A. Abdel-Rahman, A.K. Verma, A. Boutejdar, and A.S. Omar, Control of bandstop response of Hi-Lo microstrip lowpass filter using slot in ground plane, IEEE Trans Microwave Theory Tech 52 (2004), 1008–1101.
4. A. Boutejdar, A. Elsherbini, S. Amari, and A.S. Omar, A new technique to double the reject band of a low-pass filter by employing coupled C-open-loop resonators as Defected Ground Structure (DGS), Asia Pacific Microwave Conf, Bangkok, Thailand, 2007, pp. 1–4.
5. S.W. Ting, Miniaturized microstrip lowpass filter with wide stopband using double equilateral U-shaped defected ground structure, IEEE Microwave Wireless Components Lett 16 (2006), 240–242.
6. A. Boutejdar and A. Omar, A miniature 5.2-GHz bandstop microstrip filter using multilayer technique and coupled octagonal defected ground structure, Microwave Opt Technol Lett 51 (2009), 2810–2813.
7. X.Q. Chen, R. Li, S.J. Shi, Q. Wang, L. Xu, and X.W. Shi, A novel low-pass filter using elliptic shape defected ground structure, Prog Electromagn Res B 9 (2008), 117–126.
8. A. Boutejdar and A. Omar, New low-pass filter design by using compensated microstrip capacitor and coupled meander defected ground structure (DGS), Recent Patents Electrical Eng J 3 (2010), 30–34.
9. A. Neyestanak, A.L. Jolani, and F. Dadgarpour, Mutual coupling reduction between two microstrip patch antennas, Canadian Conference on Electrical and Computer Engineering (CCECE), 2008, pp. 739–742.

INVESTIGATION OF TRUNCATED WAVEGUIDES

Nathan P. Lourie,[1] David T. Chuss,[2] Ross M. Henry,[2] and Edward J. Wollack[2]
[1] Department of Physics and Astronomy, University of Pennsylvania, Philadelphia, PA 19104-6396
[2] Observational Cosmology Laboratory, NASA Goddard Space Flight Center, Greenbelt, MD 20771; Corresponding author: David.T.Chuss@nasa.gov

Received 27 September 2012

ABSTRACT: *The design, fabrication, and performance of truncated circular and square waveguide cross-sections are presented. An emphasis is placed upon numerical and experimental validation of simple analytical formulae that describe the propagation properties of these structures. A test component, a 90-degree phase shifter, was fabricated and tested at 30 GHz. The concepts explored can be directly applied in the design, synthesis and optimization of components in the microwave to submillimeter wavebands.* © 2013 Wiley Periodicals, Inc. Microwave Opt Technol Lett 55:1281–1285, 2013; View this article online at wileyonlinelibrary.com. DOI 10.1002/mop.27561

Key words: *circuit synthesis and modeling; polarization; waveguide components; eigenvalue calculation*

1. INTRODUCTION

Square and circular waveguides are commonly used in antenna feed networks for dual-polarization systems. Not only do these simple geometries lend themselves to analytical calculation but also to conventional methods of fabrication and alignment. Their high degree of symmetry enables one to achieve homogenous propagation for both polarization modes. Truncation of the guide cross-section under this condition enables the realization of broadband components for antenna applications [1], mode conversion [2–5], and polarization discrimination [6].

At times, however, it is desirable to intentionally introduce phase shifts between the two degenerate modes in the structure to alter the polarization state in this propagation environment. Differential loading (i.e., intentionally breaking the symmetry between the two propagation waveguide modes) is typically employed to achieve the desired birefringence [1]. In metallic adiabatic waveguide structures, this can be achieved through the introduction of perturbations in the guide cross-section, differentially loading the guide walls with dielectric, or subwavelength corrugations. Approaches to achieve this condition with discrete discontinuities include waveguide apertures/irises or posts separated by quarter-wave delays. Electromagnetically similar configurations with pockets, ridges, and septa can also be employed.

In going from single waveguide elements to freespace arrays of such structures, symmetry imposes a useful correspondence [7] that has led to the waveguide simulator technique [8] commonly used in the design of frequency- and polarization-selective surfaces. Examples that arise in practice include artificial dielectric layers [9, 10], quasi-optical filters [11, 12], and multilayer absorber structures [13]. From perspective of a waveguide simulator, the frequency in units of guide cutoff frequency plays the role of the reciprocal of the sine of the scan angle in the modeled response. This mapping enables physical insight into the response of such waveguide and freespace analog structures. This is particularly useful in understanding the polarization response. For example, at a finite angle of incidence, one observes that the response of a dielectric (naturally occurring or synthesized from guided-wave elements) is inherently